Fizika Nizkikh Temperatur, 2011, v. 37, No. 5, p. 551–557

Loosing thermodynamic stability in amorphous materials

Valery B. Kokshenev

Departamento de Física, Universidade Federal de Minas Gerais, Instituto de Ciências Exatas
Caixa Postal 702, CEP 30123-970, Belo Horizonte, Brazil
E-mail: valery@fisica.ufmg.br

Received December 1, 2010

The primary relaxation dynamics near the glass transformation temperature T_g exhibits universal features in all glass formers, when showing two-level tunneling states (*Low Temp. Phys*. **35**, 282 (2009)). Researchers have long searched for any signature of the underlying "true" ergodic–nonergodic transition emerging at a certain thermodynamic instability temperature T_e . Here, the relaxation timescale for glass-forming materials is analyzed within a self-consistent thermodynamic cluster description combined with the cluster percolation concept. Exploring the ergodic hypothesis, its violation is found near a crossover from the Gaussian to non-Gaussian (Poisson) cluster-volume fluctuations, describing the finite-size fractal-cluster distributions. The transformation of the compact-structure "ergodic" clusters into hole-like glassy nanoclusters is attributed to the critical-size thermal fluctuations. The ergodic–nonergodic phase diagram showing T_e is predicted in the model-independent form through the glass fragility parameter known for organic and inorganic liquids and amorphous solids. In all cases the ergodic-instability temperature is located below and close to the glass transformation temperature, whereas the distance between the two characteristic temperatures decreases with growing the material fragility.

PACS: **61.41.+e** Polymers, elastomers, and plastics;
61.43.Fs Glasses;
64.70.P– Glass transitions of specific systems.

Keywords: glass forming materials, ergodic hypothesis, thermodynamic instability.

1. Introduction

The structural transformation, which occurs under cooling rates preventing formation of the long-range crystalline order, is essentially a crossover from the high-temperature thermally equilibrated ergodic state to low-temperature nonergodic glassy states, characteristic of amorphous solids studied near the *glass transformation temperature* T_g via scanning calorimetry, e.g., [1–3]. Researchers have long searched for a signature of the underlying "true" ergodic–nonergodic transition emerging at a certain ergodic-instability temperature, designated by the critical temperature at which the certain physical characteristics exposes a divergent behavior. A traditional approach is mapping the order–disorder thermodynamic transitions onto the geometric, *cluster percolation* picture, e.g., [4].

There are several ways of description of the nontrivial ergodicity breaking in spin-glass theories. One example is the incorporation of the cluster-distribution function into a percolation free-energy by means of employing of the analogy with the Ising model [5] where the cluster distribution function exhibits a singularity near the percolation threshold [4]. It has been also recognized that in the formation of the collective order specific of metastable glassy-like states, the singularities in the cluster-size distributions are avoided, by both the asymptotically small and large clusters. It has been shown in [6] for the specific case of supercooled liquids (SCLs) that the ergodicity breaking can be developed through a dynamic crossover from the ideal-gas state to nonideal gas, characterized by the strengthening of the intermolecular correlations. Such a molecule-correlation crossover in the ergodic gas system was illuminated through the description of a smooth transformation from the Gaussian-type to Poisson-like volume-molecule fluctuations. The Gaussian-to-Poisson crossover in cluster distribution was first observed by Chamberlin *et al*. [7] in a number of SCLs, below the conventional glass transition temperature T_g through the stress relaxation data. A correlation between nonergodicity and non-Gaussianity in the glass formation process was also later discussed by Odagaki [8] and experimentally tested by Colby [9].

In the present study, the theoretical approach to the problem of the ergodic–nonergodic instability communicated in [6], is improved and extended over inorganic li-

quids and amorphous solids. Equation for T_e is re-analyzed and presented in the model-independent form that provided the ergodic instability boundary in different glass forming materials. This boundary now is tested by recent experimental data obtained for glass-forming polymers and metal alloys.

2. Background

2.1. Phenomenological and model forms

The phenomenological Vogel–Fulcher–Tammann (VFT) fitting form, namely

$$\tau_T^{(VFT)} = \tau_{\min}^{(VFT)} \exp\left(\frac{D}{\varepsilon_T}\right), \quad \text{with} \quad \varepsilon_T = \frac{T}{T_0} - 1, \quad (1)$$

which also reads as

$$\log_{10}\tau_T^{(VFT)} = \log_{10}\tau_{\min}^{(VFT)} + \frac{B}{T - T_0}, \quad \text{with} \quad B = \frac{DT_0}{\ln 10}, \quad (2)$$

is widely used to describe the non-Arrhenius temperature behavior of the structural relaxation times observed in amorphous liquids and solids; D is the so-called strength index [10,11] and T_0 is the VFT temperature. The VFT form performs within the temperature domain [12] $T_g \le T < T_c$, where T_c is the *crossover temperature* T_c between the moderately and strongly supercooled liquid states [12], distinguished in the mode coupling theory [1].

In order to characterize the timescale temperature behavior, the *timescale steepness function*

$$m_T \equiv -\frac{d\,\log_{10}\tau_T}{d\ln T} = -\frac{T}{\ln 10}\frac{d\,\ln\tau_T}{dT} \quad (3)$$

is also defined [6,12]. When applied to Eq. (1) at $T = T_g$, one arrives at the *glass-former fragility* [11]

$$m_g = m_g^*\left(1 + \frac{1}{\varepsilon_g}\right), \quad \text{with} \quad \varepsilon_g = \frac{T_g}{T_0} - 1, \quad (4)$$

where $m_g^* = m_g^{*(VFT)}$ is the material-independent lower limit, following from Eq. (1), that can be also presented in the *model-independent form* $m_g^* = \log_{10}(\tau_g^{(\exp)}/\tau_\infty^{(\exp)})$. The insertion of the estimates $\tau_g^{(\exp)} = 10^{2\pm1}$ s and $\tau_\infty^{(\exp)} = 10^{-14\pm2}$ s in Eq. (4) and m_g^* yields the well-known constraint for the characteristic-temperature ratio [13,11]

$$\frac{T_g}{T_0} = \frac{m_g}{m_g - m_g^*}, \quad m_g^* = 16 \pm 2. \quad (5)$$

The experimental validity of Eq. (5) for SCLs was tested in Fig. 2 in Ref. 12, along with similar equation

$$\frac{T_c}{T_g} = \frac{m_g + m_c^*}{m_g - m_c^*}, \quad m_c^* = 7 \pm 1, \quad (6)$$

obtained [14] for the the crossover temperature, where m_c^* is the corresponding lower fragility limit.

In the seminal *thermodynamic model* by Adam and Gibss (AG) [15], the dynamic properties of SCLs are described by

$$\tau_T^{(AG)} = \tau_{\min}^{(AG)} \exp\left(\frac{\Delta\mu^{(AG)} n_T}{k_B T}\right) \quad (7)$$

obtained through the average transition probability $1/\tau_T^{(AG)}$ characteristic of the smallest-size *cooperatively rearranging regions* (CRRs). Here $\Delta\mu^{(AG)}$ is the molar (solid-over-liquid excess) chemical potential, approximated by a constant, whereas n_T stands for the mean number of molecules which constitute the rearranging region.

The SCLs were studied [17] simultaneously on the basis of the dynamic data $\tau_T^{(\exp)}$, derived from the dielectric loss spectra, and the thermodynamical experimental data on the *configurational entropy*, namely

$$\Delta S_T = \int_{T_K}^{T} \frac{\Delta C_T}{T}\, dT, \quad \Delta C_T = C_T^{(\text{liq})} - C_T^{(\text{sol})}, \quad (8)$$

evaluated through the excess liquid-over-solid *isobaric* specific heat ΔC_T . The *thermodynamic* Kauzmann temperature [18] T_K is defined by the condition $\Delta S_K = 0$. Since the experimental fact that the high-temperature asymptote is observed as $\Delta C_T^{(\exp)} \propto T^{-1}$, the AG model was specified in both thermodynamic and dynamic aspects. Hence, the configurational entropy (8) was found [17] in the explicit *interpolation form*, namely

$$\Delta S_T^{(\text{int})} = \Delta S_\infty\left(1 - \frac{T_K}{T}\right), \quad \text{with} \quad \Delta S_\infty = \frac{C}{B}, \quad (9)$$

where B is the VFT-form dynamic parameter, defined in Eq. (2), and C is the thermodynamic parameter given in Eq. (10). Also, Eq. (7) was introduced into the AG model (see, e.g., [16]) via

$$\log_{10}\tau_T^{(AG)} = A + \frac{C}{T\Delta S_T^{(AG)}}, \text{ with} \frac{C}{\Delta S_T^{(AG)}} = \frac{\Delta\mu^{(AG)} n_T}{k_B \ln 10}. \quad (10)$$

2.2. Fluctuation mechanism of cluster formation

The idealized *isobaric* process of solid–cluster formation is defined by the variation of the Gibbs potential

$$\delta G_T^{(\text{sol})}(n, p) = -S_T^{(\text{sol})}(n)\delta T + \mu_T^{(\text{sol})}\delta n\,.$$

The cluster growth, if adopted at the thermal equilibrium temperature T_{eq} , is determined by a minimization of the total system potential that requires $\mu_{\text{eq}}^{(\text{sol})} = \mu_{\text{eq}}^{(\text{liq})}$ for the *chemical potentials* and $S_{\text{eq}}^{(\text{sol})} < S_{\text{eq}}^{(\text{liq})}$ for the *entropies*, given at $T = T_{\text{eq}}$ [19]. The stabilization of the liquid–solid boundary, when temperature drops below the equilibrium temperature, is also ensured by the minimization of compe-

ting Gibbs potential and, requiring positivity of both the excess chemical potential $\Delta\mu_T = \mu_T^{(\mathrm{sol})} - \mu_T^{(\mathrm{liq})}$ and entropy $\Delta S_T(n) = S_T^{(\mathrm{liq})}(n) - S_T^{(\mathrm{sol})}(n)$ at $T < T_{\mathrm{eq}}$. Even though the SCL system is not globally at equilibrium, it can be divided into subsystems that are almost at equilibrium with their neighbors and $\Delta S_T = = < \Delta S_T(n) >_C$ can be introduced via the configurational average

$$< ... >_C = \int_0^\infty ... P_T(n)\, dn, \tag{11}$$

through the local-equilibrium conditions.

Within the *fluctuation mechanism* adopted for the formation of spatially heterogeneous clusters, the probability $P_T(n)dn$ of meeting a solid cluster of molecular size n is that of finding the variable n lying between n and $n + dn$. This process is driven by the temperature-dependent *total system entropy*

$$S_T(n) = S_T^{(\mathrm{sol})}(n) + S_T^{(\mathrm{liq})}(n) + S_T^{(\mathrm{mix})}(n),$$

including the solid–liquid mixing term $S_T^{(\mathrm{mix})}$, passing through the maximum at $n = n_T$, in the quasi-static approximation. The maximum-entropy principle [19] provides the probability density

$$P_T(n) = \exp\left[\frac{S_T(n)}{k_B}\right] \sim \exp\left[-\frac{(n-n_T)^2}{2\Delta n_T^2}\right], \tag{12}$$

where the mean glassy-cluster molecular size n_T is established by the thermodynamic conditions of the cluster contact with the thermal bath of temperature T_{eq}. The *cluster-size fluctuation* is introduced by

$$\Delta n_T^2 = < (n - n_T)^2 >_C \; = \; -\left(\partial^2 S_T / k_B \partial n^2\right)^{-1}_{n=n_T},$$

emerging in Eq. (12), that is expected to work beyond the equilibrium.

The clusters of molecular size n appear and disappear from a fluid volume with *frequency* $\tau_T^{-1}(n)$, where $\tau_T(n)$ is lifetime of a given *n*-cluster. The probability of rearrangement of such kind of clusters is given by $\tau_T^{-1}(n)$ determined by the maximum of the boundary-formation entropy $\Delta S_T(n)$ established at the mesoscopic size-scale, namely

$$\tau_T^{-1}(n) = \tau_{\min}^{-1} \exp\left[\frac{\Delta S_T(n)}{k_B}\right] = \tau_{\min}^{-1} \exp\left[-\frac{W_{\min}(n)}{k_B T_{\mathrm{eq}}}\right]. \tag{13}$$

Here $W_{\min} = \Delta G_T(n)$ corresponds to the *minimum work* required for solidification of n molecules driven by cluster-size fluctuations [19]. Within the adopted isobaric-isothermal mechanism, one has

$$\Delta G_T(n) = n\left[\mu_T^{(\mathrm{sol})} - \mu_{\mathrm{eq}}^{(\mathrm{liq})}\right].$$

Consequently, Eq. (13) can be extended to supercooled $(T < T_{\mathrm{eq}})$ states through the relation

$$\tau_T(n) = \tau_a' \exp\left(\Delta\mu_T n / k_B T\right),$$

introducing cluster relaxation time on the *mesoscopic time-scale* $\tau_T \equiv < \tau_T(n) >_C$, whereas $n_T \equiv < n >_C$.

In the simplest case of $n \equiv n_T$, when clusters-size fluctuations are ignored, one naturally arrives at pseudo-Arrhenius form

$$\tau_T^{(VFT)} = \tau_{\min}^{(VFT)} \exp\left(E_T / k_B T\right),$$

with $E_T = \Delta\mu_T n_T$, following from the VFT and AG forms presented in Eqs. (1) and (7). When the Gaussian fluctuations are large ($\Delta n_T > n_T$), the extension of the Arrhenius form via Eq. (13), namely

$$\tau_T^{(\mathrm{mod})} = \tau_a \exp\left[\frac{E_T}{k_B T}\left(1 + \frac{\Delta E_T}{2k_B T}\right)\right], \tag{14}$$

results in a high-temperature thermodynamic perturbation series for the primary relaxation scale [12].

When the *mode coupling theory* (MCT) [1] is extended by the energy fluctuations ΔE_T [20], one obtains

$$\tau_T^{(MCTe)} = \tau_a \left[\exp\left(1 + \frac{\Delta E_T}{2k_B T}\right)\right]^{\frac{E_T}{k_B T}} \propto \frac{\tau_\infty^{(MCT)}}{\left(1 - \frac{T_c}{T}\right)^{\gamma_c}}, \text{ for } T \gg T_c, \tag{15}$$

from Eq. (14) providing asymptotically the known MCT extrapolation form [1]. When the thermal fluctuations of CRRs are taken into consideration, the extended version of the AG theory was introduced [20] as

$$\tau_T^{(AGe)} = \tau_a \exp\left[\frac{\Delta\mu_g n_a}{k_B T_0 \varepsilon_T}\left(1 + \frac{1}{\gamma_c}\frac{\Delta\mu_g n_a}{k_B T_0 \varepsilon_T}\right)\right], \tag{16}$$

where n_a is the lower limit for the CRR number n_T. One can see that both dynamic and thermodynamic forms are linked by the MCT *slowing down exponent* γ_c, lying in the range [12] $2 \le \gamma_c^{(\exp)} < 3$ for SCLs and $3 \le \gamma_c^{(\exp)} < 4$ for glass-forming polymers. Also, the ratio for the excess chemical potentials was obtained (see Eq. (37) in [12]), namely

$$\frac{\Delta\mu_g}{\Delta\mu_c} = \frac{\varepsilon_g}{4\varepsilon_c}\left(\sqrt{1 + 8\frac{m_g^*}{\gamma_c}\ln 10} - 1\right), \tag{17}$$

where $m_g^* = 16 \pm 2$ is the model-independent parameter.

3. Thermodynamic instability

3.1. Ergodic versus nonergodic version

Exploring a minimum set of the observable parameters in glass-forming materials, i.e., T_0, T_g, m_g, T_c, and γ_c,

the *ergodic A*-version for self-consistent description of the primary timescale $\tau_T^{(\exp)}$, its steepness $m_T^{(\exp)}$, and curvature $\varkappa_T^{(\exp)}$ [20] can be introduced. Specifically, the high-density solid-like ergodic clusters are presented in Eq. (16) by relation times $\tau_T^{(A)} \equiv \tau_T^{(AGe)}$. Even though the global equilibrium is not achievable in SCLs, the ergodic hypothesis has been in fact implicitly employed via the Gaussian cluster distribution $P_T^{(A)}(n)$ (12), providing the thermodynamic description for long-living metastable states. In other words, it is suggested that thermodynamic macroscopic observables evaluated above T_e in the thermodynamic limit $N \to \infty$ can be well approximated by corresponding statistical quantities estimated in the static limit $t \to \infty$.

In order to describe $\tau_T^{(\exp)}$ below T_e, the low-density solid-like clusters are introduced via a *nonergodic B*-version, with the help of non-Gaussian distribution

$$P_T^{(B)}(n) \sim \exp\left[-\frac{1}{\sigma}\left(\frac{n}{\zeta_T}\right)^{\sigma}\right], \; T_0 < T \le T_e, \qquad (18)$$

presented by the Stauffer cluster scaling form [21] taken in the simplest large-cluster approximation. Here $\zeta_T = \zeta_b \varepsilon_T^{-1/\sigma}$ stands for the typical cluster molecular size, always exceeding ζ_b, and ε_T is given in Eq. (1). The standard method of steepness descent results in the late-time primary relaxation given by

$$\tau_T^{(B)} = \tau_a \exp\left[\left(\frac{\sigma-1}{\sigma}\right)\varepsilon_T \left(\frac{\Delta\mu_b \zeta_b}{k_B T \varepsilon_T}\right)^{\frac{\sigma}{\sigma-1}}\right] \qquad (19)$$

obtained for large and stable clusters ensured, respectively, by the saddle-point conditions $\sigma > 1$ and $\sigma \ge 2$. Aiming to design a new nonergodic VFT–AG fitting form in terms of the percolation-type clusters specified by $\sigma = 2$, Eq. (19) is reduced to

$$\tau_T^{(B)} = \tau_a \exp\left(\frac{\Delta\mu_b^2 n_b}{2k_B^2 T^2 \varepsilon_T}\right) \approx \tau_a \exp\left(\frac{D_e^{(B)}}{\varepsilon_T}\right), \text{ for } T_0 < T \le T_e, \qquad (20)$$

where $n_b = \zeta_b^2$ and a new strength index $D_e^{(B)} = \Delta\mu_b^2 n_b / 2(k_B T_e)^2$ defined at T_e. Thus, Eq. (18) emerges as a pseudo-Gaussian form with $\Delta n_T^2 = n_T^{(B)} \equiv n_b \varepsilon_T^{-1}$.

The proposed distribution $P_T^{(B)}$ provides a description of the *A*–*B*-state crossover which is thought of as a *smooth* cluster structure rebuilding at T_e. We therefore define continuous changes in the cluster molecular size and variance via $n_e^{(A)} = n_e^{(B)}$ and $\Delta n_e^{(A)} = \Delta n_e^{(B)}$. The variance closely related to the cluster structure exhibits a kink [20], when it transforms from

$$\Delta n_T^{(A)} = \xi_c n_T^{(A)} = \xi_c n_a / (1 - T_0 / T)$$

into

$$\Delta n_T^{(B)} = \sqrt{n_b}\, \varepsilon_T^{-1/2} = \zeta_b / \sqrt{T / T_0 - 1}.$$

Accounting for these relations, the conditions of cluster continuous changes yield

$$T_e = T_0 \frac{n_b}{n_a} = \frac{T_0}{1 - \xi_c^2 n_a^2}, \qquad (21)$$

where $\xi_c = \sqrt{2/\gamma_c}$. Also, the condition of continuity for the strength indexes, i.e., $D_e^{(A)} = D_e^{(B)}$, where $D_e^{(A)} = D_e^{(AGe)}$ is established with the help of Eq. (16), taken at $T = T_e$, provides

$$\frac{\Delta\mu_g n_a}{T_0}\left(1 + \frac{1}{\gamma_c}\frac{\Delta\mu_g n_a}{k_B T_0 \varepsilon_e}\right) = \frac{\Delta\mu_0^2 n_b}{2k_B T_e^2}. \qquad (22)$$

Here the metastable states A and B are energetically distinguished through their chemical potentials $\Delta\mu_T$, approximated by constants within the corresponding domains: $\Delta\mu_T^{(A)} = \Delta\mu_a = \Delta\mu_g$, for $T_e \le T < T_c$, but $\Delta\mu_T^{(A)} = \Delta\mu_c$, when $T \ge T_c$; $\Delta\mu_T^{(B)} = \Delta\mu_b = \Delta\mu_0$, for $T_0 < T \le T_e$. Then, employing Eq. (21), one obtains the relations $\Delta\mu_c n_a = \gamma_c \varepsilon_c T_0$ and $\Delta\mu_c = 2\varepsilon_c T_0 / \xi_c^2 n_a = 2\varepsilon_c T_e / \varepsilon_e$, reducing Eq. (22) to

$$T_e = T_0 + (T_c - T_0)\Lambda_\mu, \; \Lambda_\mu = \frac{\Delta\mu_0^2 - \Delta\mu_g^2}{\Delta\mu_c \Delta\mu_g}, \text{ with } T_0 < T_e < T_c. \qquad (23)$$

To find ratios between the AGe chemical potentials involved in Eq. (23), one needs to parametrize the observed fragility data $m_g^{(\exp)}$ through the steepness functions $m_T^{(A)}$ $(= m_T^{(AGe)})$ and $m_T^{(B)}$, obtained at T_g and *extrapolated* to T_g, via the corresponding model versions $\tau_T^{(A)}$ (16) and $\tau_T^{(B)}$ (20).

As seen in Eq. (17), the AGe timescale parametrization involves, besides the chemical potentials, the slowing down exponent $\gamma_c^{(A)}$. This allows one to reformulate the timescale fitting problem as follows. Instead of the observation of fragility through the equations $m_g^{(A)} = m_g^{(\mathrm{mod})} \approx m_g^{(B)}$ with $m_g^{(\mathrm{mod})} = m_g^*(1 + \varepsilon_g^{-1})$, we describe the experimental data on $\gamma_c^{(\exp)}$, within the framework of the A and B scenarios. They are introduced by the estimates

$$\gamma_c^{(A)} = m_g^* \ln 10 \left[\frac{\Delta\mu_g}{\Delta\mu_c}\frac{\varepsilon_c}{\varepsilon_g}\left(1 + 2\frac{\Delta\mu_g}{\Delta\mu_c}\frac{\varepsilon_c}{\varepsilon_g}\right)\right]^{-1} \qquad (24)$$

and

$$\gamma_c^{(B)} = m_g^* \ln 10 \left[\left(\frac{\Delta\mu_e}{\Delta\mu_c}\right)^2 \frac{\varepsilon_c^2}{\varepsilon_g \varepsilon_e}\left(\frac{T_e}{T_g}\right)^2 \left(1 + 2\frac{m_g^*}{m_g}\right)\right]^{-1}, \qquad (25)$$

obtained through $m_g^{(A)}$ and $m_g^{(B)}$, calculated by steepness m_T (3) at $T = T_g$ on the basis of corresponding $\tau_T^{(A)}$ (16) and $\tau_T^{(B)}$ (20).

In Fig. 1, the numerical analysis of the model predictions in Eqs. (24) and (25) is provided where unknown

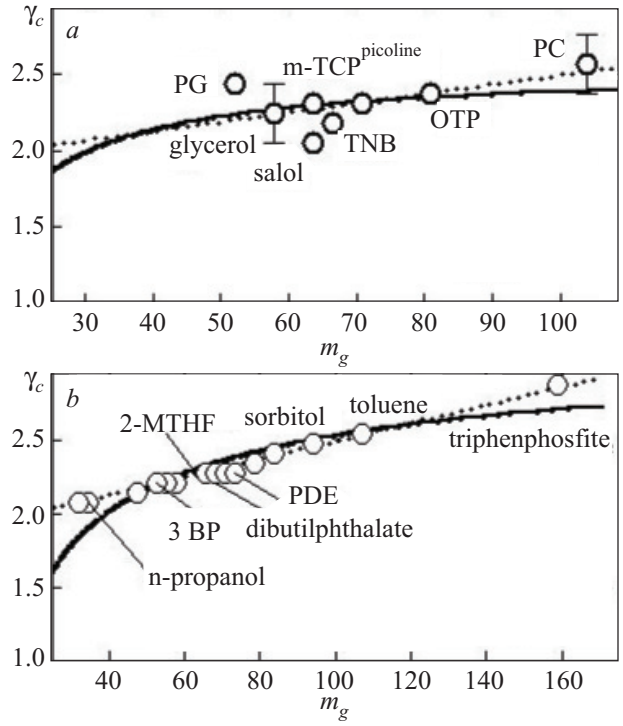

Fig. 1. Observation of the data on the slowing-down exponent in SCLs through the ergodic (*a*) and nonergodic (*b*) versions for the glassy-like solid clusters. *a* — The points are available experimental data on $\gamma_c^{(\exp)}$ taken from Table 1 in Ref. 12. The bars indicate experimental error. The dotted line is the best linear fit of the data. The solid line is drawn through Eq. (24), with $m_g^* = 16$ and the fitting parameter $\Delta\mu_g / \Delta\mu_c = 1.32$. *b* — The dotted line is the same as in *a*. Points are model predictions for the slowing-down exponent $\gamma_c^{(\mathrm{mod})}$ through Eq. (25). The solid line is drawn through Eqs. (23) and (25), with $m_g^* = 16$, $\Delta\mu_g / \Delta\mu_c = 1.32$, and the overall fitting parameter $\Delta\mu_0 / \Delta\mu_c = 1.47$.

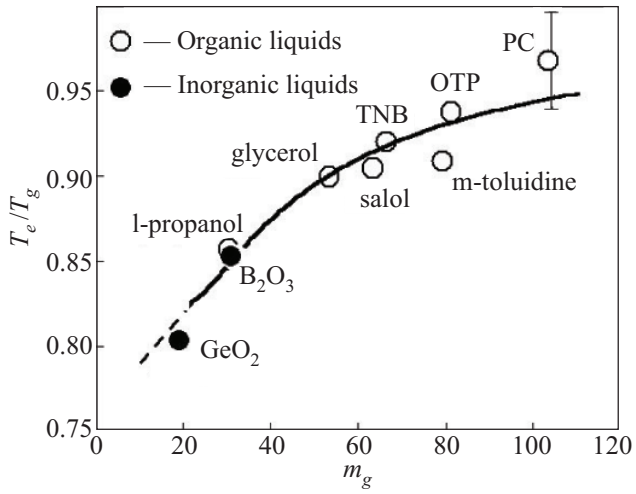

Fig. 2. Observation of the ergodic–nonergodic crossover in supercooled liquids. The solid line is the glass crossover temperature T_e reduced by T_g, shown in Eq. (26). The dashed line is a linear interpolation of Eq. (26) to the strong-glass SCL regimes. The points, taken from Table 1 of Ref. 22, are the outcome of the fitting analysis [22] of the data on dielectric loss, viscosity, and mechanical shear relaxation in low molecular weight organics (open circles) and inorganic (closed circles) SCLs.

temperature T_e in $\gamma_c^{(A)}$ and $\gamma_c^{(B)}$ is excluded by means of Eq. (23).

The observation in Fig. 1 of the experimental data $\gamma_c^{(\exp)}$ for the SCLs through the relations $\gamma_c^{(A)} = \gamma_c^{(\exp)} \approx \gamma_c^{(B)}$ results in the model estimates $\Delta\mu_g / \Delta\mu_c = 1.32 \pm 0.05$ and $\Delta\mu_0 / \Delta\mu_c = 1.47 \pm 0.06$.

3.2. Observation of the ergodic–nonergodic crossover

The obtained in Fig. 1 estimates for the chemical potentials of solid-like clusters in SCLs provide $\Lambda_\mu^{(SCL)} = 0.317$ in Eq. (23) for *glass crossover temperature* $T_e^{(SCL)}$. Being numerically close to $1/3$, this result supports another estimate $T_e^{(SCL)} = (2T_0 + T_c)/3$ discussed in Eq. (42) in Ref. 12. Here, we specify Eq. (23) via Eqs. (5) with $m_g^* = 16$ and Eqs. (6) with $m_c^* = 7$, via a new prediction

$$\frac{T_e^{(SCL)}}{T_g} = \frac{m_g^2 - 13.5 m_g + 76.5}{m_g (m_g - 7)} \qquad (26)$$

now extended from organic to inorganic liquids.

In Fig. 2, Eq. (26) is analyzed in light of the data on the critical temperature T_c, proposed earlier by Colby [9], which signals the dynamic instability below T_g associated here with glass transition temperature T_e. Taking also into consideration that no adjustable parameters are used in Fig. 2, we infer that the critical behavior observed in the dynamic experiments in SCLs [9,22] originates from the loss of ergodicity below T_g, firstly reported in Ref. 23 and then explained in Ref. 6. Despite of the fact that the employed AGe model is limited by "regular" liquids, Eq. (26) also includes salol, as follows from the analysis in Fig. 2. This implies that during the A–B crossover, differently distributed clusters expose a similar, model-independent behavior. In other words, the smallest glassy-like clusters, which emerge near T_e, have a gas-like structure [6], regardless of the underlying chemical potentials and geometry. Likely the same refers to the glassy-cluster-size fluctuations, which distinguish the "regular" and "irregular" liquids above T_e discussed in Ref. 12.

These observations suggest application of general Eq. (23) to other glass-forming materials, where Λ_μ is treated as a generic parameter. In Fig. 3, the special case of polymers is presented by

$$\frac{T_e^{(\mathrm{pol})}}{T_g} = \frac{m_g^2 - 12.5 m_g + 72.8}{m_g (m_g - 7)}. \qquad (27)$$

For the case of spin-glass forming metallic alloys, a similar analysis was elaborated on the basis of kinetic data

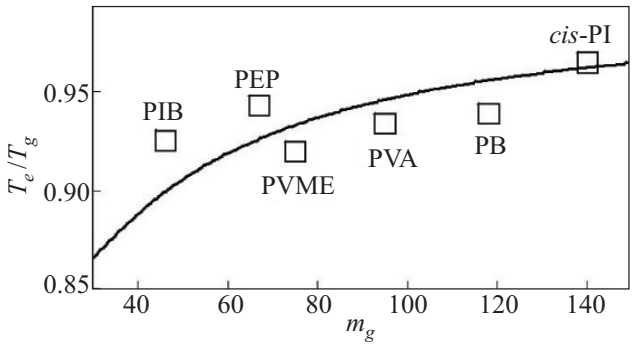

Fig. 3. Observation of the ergodic–nonergodic crossover in glass-forming polymers. The points are provided from Table 1 in Ref. 22. The line is Eq. (23) taken with $\Lambda_{\mu}^{(\mathrm{pol})} = 0.350$ for best fit and represented in the fragility-variable form in Eq. (27).

on the relaxation timescale [9]. One finds $\Lambda_{\mu}^{(\mathrm{met})} = 0.285$, using the i) data on the critical temperature shifts $\Delta T_c = T_g - T_c$, with $T_c = T_e$, observed [9] as 75 and 72 K for two alloys $Pd_{48}Ni_{32}P_{20}$ and $Pt_{60}Ni_{15}P_{25}$, having the common fragility $m_g = 48$, and ii) the data [24] on the glass transformation temperature $T_g =$ 566 and 482 K, respectively. In turn, the generic parameter for metallic alloys results in the prediction for *glass crossover temperature*

$$T_e^{(\mathrm{met})} = T_g \frac{m_g^2 - 14.5 m_g + 80.1}{m_g (m_g - 7)} \qquad (28)$$

illustrated in Fig. 4.

4. Conclusion

We have discussed the problem of the true thermodynamic instability occurring during structural glass and spin-glass transformation in glass forming materials presented here by molecular, polymeric supercooled liquids and metallic alloys, respectively. It has been repeatedly demonstrated that a generalized solution to the glass formation process in microscopically different systems is possible, if designed on mesoscopic level. Although a unique coherent theoretical framework remains a challenge, the proposed complex geometric, dynamic and thermodynamic approach to the problem offers novel relations between the observable dynamic exponents and thermodynamic and kinetic macroscopic parameters. A *macroscopic parametrization* of the primary timescale, made in a self-consistent manner, provides a strong evidence for mutual dependence between thermodynamic (T_0 and T_g) and dynamic (T_c) characteristic temperatures [12,14] as well as ergodic–nonergodic temperature [6] T_e. In this study, we have improved analysis of the critical temperature T_e presenting it in the model-independent form that allowed one to extend the applications from the glass-forming organic and inorganic liquids over polymers and metallic glasses. All predicted crossover glass temperatures indicate that the distance between the two characteristic temperatures T_g and T_e decreases when the glass material fragility grows, implying that true glass transition near the glass transition temperature T_g can be expected only in the very strong glass formers.

Finally, the proposed approach can be extended over traditional quadrupolar orientational glasses and modern dipolar orbital glasses, for which microscopic description is developed in Refs. 25 and 26, respectively. For these cases, an evaluation of the ergodic–nonergodic instability boundary is though limited by the absence of systematic data on the characteristic temperatures and slowing-down exponents discussed in Eqs. (23)–(25).

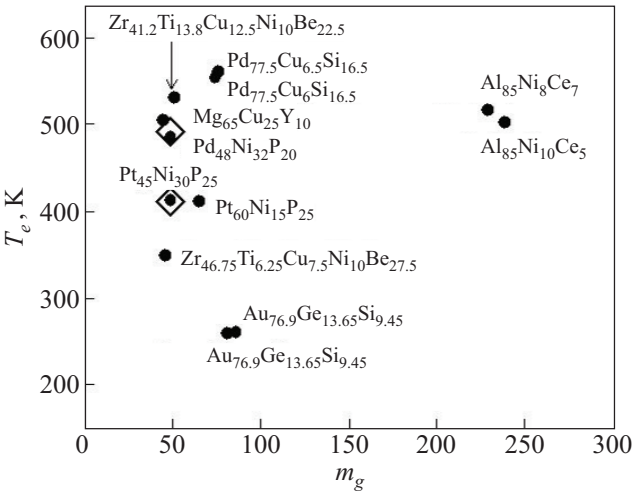

Fig. 4. Glass crossover temperatures in metallic alloys against fragility. The closed circles are estimated through Eq. (28), with the known T_g and m_g, taken from Table 1 in Ref. 24. The open diamonds indicate two alloys studied by Colby [9] and discussed in the text.

Acknowledgments

The financial support by CNPq and FAPEMIG is acknowledged.

1. W. Götze and L. Sjögen, *Rep. Prog. Phys.* **55**, 241 (1992).
2. C.A. Angell, K.L. Ngai, G.B. McKenna, P.F. McMillan, and S.W. Martin, *J. Appl. Phys.* **88**, 3113 (2000).
3. V.B. Kokshenev, *Heterostructured Molecular Clusters in Supercooled Liquids and Other Glass-Forming Materials: Dynamic and Thermodynamic Appearance in the Primary Structural Relaxation*, Chapter in *Atomic and Molecular Cluster Research*, Y.L. Ping (ed.), Nova Science Publishers, Inc. N.Y. (2006).
4. M.B. Isichenko, *Rev. Mod. Phys.* **64**, 961 (1992).
5. H. Kunz and B. Souillard, *Phys. Rev. Lett.* **40**, 133 (1978).
6. V.B. Kokshenev, *Solid State Commun.* **119**, 429 (2001).
7. R.V. Chamberlin, R. Böhmer, E. Sanchez, and C.A. Angell, *Phys. Rev.* **B46**, 5787 (1992).
8. T. Odagaki, *Progr. Theor. Phys. Suppl.* **126**, 9 (1997).
9. R.H. Colby, *Phys. Rev.* **E61**, 1783 (2000).

10. R. Böhmer, K.L. Ngai, C.A. Angell, and D.J. Plazek, *J. Chem. Phys.* **99**, 4201 (1993).
11. R. Böhmer and C.A. Angell, *Phys. Rev.* **B48**, 5857 (1993).
12. V.B. Kokshenev, P.D. Borges, and N.S. Sullivan, *J. Chem. Phys*. **122**, 114510 (2005).
13. R. Böhmer and C.A. Angell, *Phys. Rev.* **B45**, 10 091 (1992).
14. V.B. Kokshenev, *Physica* **A262**, 88 (1999).
15. J.H. Gibbs and G. Adam, *J. Chem. Phys.* **43**, 139 (1965).
16. V.B. Kokshenev, *Fiz. Nizk. Temp.* **35**, 371 (2009) [*Low Temp. Phys.* **35**, 286 (2009)].
17. R. Richert and C.A. Angell, *J. Chem. Phys.* **108**, 9016 (1998).
18. W. Kauzmann, *Chem. Rev.* **43**, 219 (1948).
19. L.D. Landau and E.M. Lifshitz, *Statistical Physics*, Pergamon Press: London (1989).
20. V.B. Kokshenev, *J. Non-Cryst. Solids* **352**, 3380 (2006).
21. D. Stauffer and A. Aharony, *Introduction to Percolation Theory*, 2nd ed.; Taylor and Francis: London (1992).
22. B.M. Erwin and R.H. Colby, *J. Non-Cryst. Solids* **307**, 225 (2002).
23. J. Colmenero, A. Alegria, A. Arbe, and B. Frick, *Phys. Rev. Lett.* **69**, 478 (1992).
24. Y. Zhao, X. Bian, K. Yin, J. Zhou, J. Zhang, and X. Hou, *Physica* **B349**, 327 (2004).
25. V.B. Kokshenev, *J. Low Temp. Phys.* **104**, 1 (1996).
26. V.V. Dmitriev, D.A. Krasnikhin, N. Mulders, A.A. Senin, G.E. Volovik, and A.N. Yudin, *JETP Lett.* **91**, 599 (2010).